Vol. 17, No. 2 (2018) 455-462
Revista Mexicana de Ingeniería Química

FACILE SYNTHESIS OF LOW BAND GAP ZnO MICROSTRUCTURES

SÍNTESIS SENCILLA DE MICROESTRUCTURAS DE ZnO DE BAJO BAND GAP

V.M. Ovando-Medina[1]*, L. Farías-Cepeda[2], N.V. Pérez-Aguilar[2], J. Rivera de la Rosa[3], H. Martínez-Gutiérrez[4], A. Romero Galarza[2], E. Cervantes-González[1], N. Cayetano-Castro[4]

[1]*Ingeniería Química, Coordinación Académica Región Altiplano (COARA) Universidad Autónoma de San Luis Potosí, Carretera a Cedral KM 5+600, San José de las Trojes, Matehuala, SLP, México 78700.*

[2]*Facultad de Ciencias Químicas, Departamento de Ingeniería Química, Universidad Autónoma de Coahuila, Blvd. V. Carranza e Ing. José Cárdenas V. S/N, Saltillo, Coah, 25280.*

[3]*Facultad de Ciencias Químicas, Universidad Autónoma de Nuevo León, Av. Universidad, Cd. Universitaria, San Nicolás de los Garza, NL, México 66451.*

[4]*Instituto Politécnico Nacional-CNMN, Luis Enrique Erro S/N, D.F., México 07738.*

Received August 28, 2017; Accepted January 30, 2018

Abstract

In this work a simple chemical route was employed to synthesize ZnO microparticles by precipitation from aqueous solution of $ZnCl_2$ as precursor, NaOH as oxidizing and sodium dodecyl sulfate (SDS) as surfactant. Samples of ZnO microparticles were analyzed by scanning electron microscopy (SEM), FTIR spectroscopy, Raman spectroscopy, X-Ray diffraction, UV/Vis-NIR diffuse reflectance, high resolution transmission electron microscopy (HR-TEM), and N_2 adsorption-desorption. It was observed from SEM analysis that ZnO microparticles with morphologies resembling six-blade impeller with diameters in the range of 500 nm to 1 m, and sheet-like (approximately 200 nm × 300 nm) were obtained through this technique. X-Ray diffraction and Raman analyses confirmed the obtaining of hexagonal wurtzite ZnO crystal structure. The calculated band gap energy was 3.19 eV, which is slightly lower than the average value reported in the literature. Specific BET area of ZnO microparticles was 26.5 m^2/g.

Keywords: ZnO, microstructures, band gap energy, SEM, morphology.

Resumen

En este trabajo se empleó un a ruta química sencilla para sintetizar micropartículas de ZnO mediante precipitación en solución acuosa de $ZnCl_2$ como precursor, NaOH como oxidante y dodecil sulfato de sodio (SDS) como tensoactivo. Las muestras de ZnO fueron analizadas mediante microscopía de barrido electrónico (SEM), espectroscopía de FTIR, espectroscopía Raman, difracción de rayos-X, reflectancia difusa de UV/Vis-NIR, microscopía de transmisión de electrones de alta resolución (HR-TEM), y mediante adsorción-desorción de N_2. Se observó mediante análisis de SEM que mediante esta técnica se obtienen micropartículas de ZnO con morfologías similares a impulsores de seis-aspas con diámetros entre 500 nm y 1 m, morfologías tipo-hojas (de aproximadamente 200 nm × 300 nm). Los análisis de difracción de rayos-X y de Raman confirmaron la obtención de ZnO con estructura cristalina wurtzita hexagonal. La energía de band gap calculada fue de 3.19 eV, la cual es ligeramente menor que el valor promedio reportado en la literatura. El área superficial BET de las nanopartículas de ZnO fue de 26.5 m^2/g

Palabras clave: ZnO, microestructuras, energía de band gap, SEM, morfología.

1 Introduction

The synthesis of semiconducting materials in the nano/micrometric scale have attracted much attention in the last decades due to their different electronic, structural, and thermal properties compared with the bulk scale, which permits to be applied as photocatalyst, sensors, electronic devices (Kumar *et al*., 2013), or in areas as medicine, agriculture, energy storage, communications, etc. (Grillo *et al*., 2015; Pereira *et al*,. 2014). ZnO is one of the most versatile materials, typical bulk uses of ZnO are as an additive in the production of diverse materials, such as plastics, ceramics, glass, adhesives, coatings, creams, foods, sunscreens, as well as bactericide and others (Bamiduro *et al*. 2014; Zamiri *et al*. 2012; Pérez-Sicairos *et al*. 2016). The importance of ZnO arises from its properties of nanostructured forms of this

* *Corresponding author. E-mail*: ovandomedina@yahoo.com.mx
doi: 10.24275/10.24275/uam/izt/dcbi/revmexingquim/2018v17n2/Ovando ; *issn-e*: 2395-8472

wide band gap (3.37 eV) semiconductor which may be exploited in electronic and photonic applications (Romo *et al*., 2011).

Particles of ZnO have a great advantage to be added to a catalytic reaction process due to their relative high specific surface area and high catalytic activity (Chen and Tang, 2007). Zinc oxide can be synthesized in one-, two-, and three-dimensional structures. One-dimensional morphologies make up the major group, for example nanorods (Banerjee *et al*., 2003), needles (Wahab *et al*., 2007), helixes, springs and rings (Kong *et al*., 2004), tubes (Wu *et al*., 2002), or -wires (Nikoobakht *et al*., 2013), among others. ZnO can be obtained in 2D structures as nanoplates and nanosheet (Chiu *et al*., 2010). Three-dimensional structures of zinc oxide comprise cauliflower, dandelion, snowflakes, spheres, etc. ZnO provides one of the greatest diversity particle structures among all known nanomaterials (Kolodziejczak-Radzimska and Jesionowski, 2014).

It has been demonstrated that zinc oxide shows different physical and chemical properties depending on the shape and sizes of nanostructures (Kumar *et al*., 2013); therefore, different methods of synthesis are being investigated with respect to the morphology, physical and chemical properties of synthesized zinc oxide. For example, Peng *et al*. (2010a, 2010b) synthesized ZnO nanostructures with star-like, tetrapod and multipod-like morphology through thermal evaporation method using Zn metal as precursor, founding that ZnO particles were about 2 μm in size, depending on the deposition temperature. Though authors named these particles as nanostructures, the sizes imply that microstructure classification is more adequate. ZnO particles have been obtained by hydrothermal process, as reported by Li *et al*. (2011) that used a complex method called hydrothermal micro continuous-flow synthesis. They used zinc acetate as precursor and NaOH as oxidant to precipitate ZnO particles. These authors observed that spherical, cylinder-, star- and flower-like ZnO particles with diameters in the range of 428 nm to 1.5 μm can be obtained, which depend upon the molar ratio of zinc acetate and NaOH.

Xie *et al*. (2011) reported a simple fabrication method to obtain ZnO particles with different morphology using $ZnCl_2$ as precursor, NaOH or LiOH as oxidant, and SDS or sodium dodecyl benzene sulfonate (SDBS) as surfactants. They studied the ZnO photocatalytic activity against methyl orange dye degradation. They observed that morphology and particles sizes depend on the ZN_2^+/OH^- molar ratio and on the surfactant type used. When using NaOH, particles acquired rod-, needle- or flower-like structure with lengths between 2 m and 15 m, and 500 nm to 780 nm in width; however by using LiOH rugby-like morphology was observed with 70 nm in length and 42 nm in width.

In this work we have synthesized ZnO microparticles with low band gap and with a mixture of morphologies resembling six-blade impeller, sheet-like and spheres by a simple chemical route. ZnO was fully characterized by SEM, HRTEM, XRD, EDS, FTIR, Raman spectroscopy, and the band gap energy was calculated by UV/Vis-NIR diffuse reflectance.

2 Materials and methods

2.1 Materials

$ZnCl_2$ (> 97%), NaOH (> 97%) and SDS (> 99%) were purchased from Jalmek (San Nicolas de los Garza, Mexico). Distilled grade water was used in the synthesis and purification.

2.2 Synthesis of ZnO nanostructures

ZnO was precipitated from aqueous solution of $ZnCl_2$. 8.17 g of $ZnCl_2$were dissolved in 60 ml of distilled water under magnetic stirring at 60 °C. Afterwards, a solution of 0.86 g of SDS dissolved in 15 ml of distilled water was added to $ZnCl_2$ solution with magnetic stirring at room temperature (25 °C ± 2 °C). After 5 min of stirring, a NaOH aqueous solution (14.4 g of NaOH in 90 ml of water) was added drop by drop under magnetic stirring. Then, 135 ml of distilled water were added to reaction mixture, and reaction proceeded through 1.5 h. After that, reaction mixture was transferred to a 500 ml glass bottle screw-top, sealed and placed in an oven at 80 °C by 5 h. ZnO product formed as a white dust at the bottom of the jar, therefore the supernatant was decanted, and ZnO product was washed several times with water using a filter paper, to remove surfactant, and other impurities. Washed ZnO was dried at 60 °C through 24 h.

2.3 Characterization

The resulting dried ZnO microparticles were analyzed by FTIR spectroscopy (Agilent, Cary 630) and Raman spectroscopy (B& W TEK INC.). SEM analysis was completed (JEOL high resolution scanning electron

microscope, JSM 7800F in SEM mode at 30 kV of beam acceleration) dispersing samples (1:100) in distilled water in the presence of ultrasound. A drop of the dispersed sample was poured onto a copper grid coated with Formvar^{TM} resin and carbon film, afterwards it was allowed to dry overnight at room temperature. ZnO was analyzed by HR-TEM (JEOL, JEM ARM 200F) at 200 kV. Elemental analysis was performed by Energy Dispersive X-Ray Spectroscopy (EDS) using a detector coupled to the SEM. X-Ray diffraction analysis (XRD) was performed with a PANalytical Empyrean diffractometer using the Cu Kα radiation (λ = 1.54056 Å) at 40 kV and 40 mA with a 2Θ step of 0.026° and a counting time of 0.4 s per point. The crystallite structure was refined via Rietveld method by use of the Topas4 code. UV/Vis-NIR diffuse reflectance spectroscopy measured between 200 and 800 nm using a spectrophotometer (Thermo Scientific, Evolution 220) equipped with an integrating sphere. The specific surface area (A_{BET}) of ZnO was determined by N_2 physisorption (Micromeritics, ASAP 2020) using the Brunauer, Emmett, Teller (BET) method.

3 Results and discussion

The reaction of zinc ions and sodium hydroxide proceeds according to equation (1):

$$ZnCl_2(aq) + 2Na(OH)(aq) \rightarrow 2Na^+ + 2Cl^- + Zn(OH)_2 \downarrow \quad (1)$$

The final product of the process is zinc oxide upon calcination by the following reaction:

$$Zn(OH)_2 \rightarrow ZnO + H_2O \quad (2)$$

Fig. 1 shows the Raman spectra of synthesized ZnO microparticles. The main peaks of ZnO at 97, 330, 380, 432, 484 and 580 cm^{-1} can be observed. Signal at 97 cm^{-1} is due to E2 low optical phonon, peak at 330 cm^{-1} represents second order Raman spectrum due to zone-boundary phonons of hexagonal ZnO (multiple phonon scattering process), signal at 380 cm^{-1} corresponds to A1 (TO) mode, peaks at 432 and at 484 cm^{-1} is ascribed to E2 high mode of non-polar optical phonon of wurtzite ZnO, and the signal at 580 cm^{-1} can be attributed to E1 (LO) mode of hexagonal ZnO (Peng *et al*. 2010a, 2010b; Filali *et al*. 2015). Fig. 2 shows the FTIR spectra of ZnO microstructures, it can be observed that the typical signal of ZnO

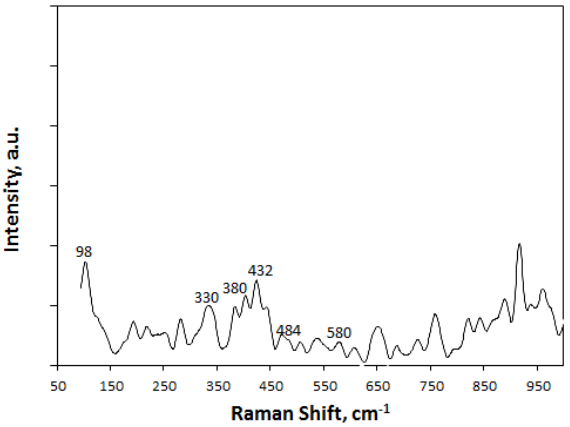

Fig. 1. Raman spectrum of ZnO microstructures.

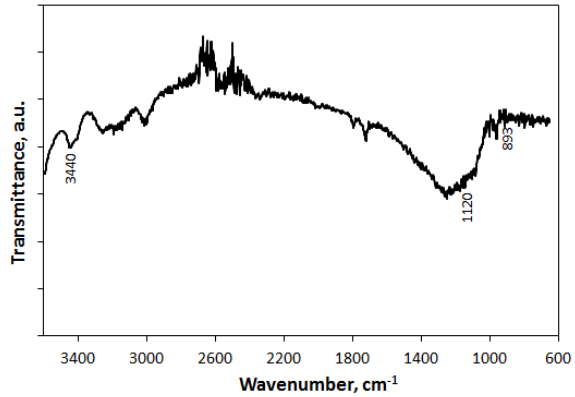

Fig. 2. FTIR spectrum of ZnO microstructures.

interaction in stretching mode was near to 893 cm^{-1} (Ovando-Medina *et al*. 2015). Metal oxides generally present signals in the fingerprint region (< 1000 cm^{-1}) due to inter-atomic vibrations. The peak observed at 3440 and 1120 cm^{-1} may be due to O-H stretching and deformation, assigned to water adsorption on the metal surface (Kumar and Rani, 2013).

Fig. 3 shows a Rietveld refinement plot from X-Ray diffraction pattern of ZnO microparticles. Diffraction peaks indicate the nanocrystalline nature. Diffraction peaks corresponding to the precursors ($ZnCl_2$ or NaOH) were not found in the XRD patterns, confirming the high purity of the synthesized ZnO. Signals at 2θ of 31.7, 34.3, 36.2, 47.5, 56.5, 62.8, 66.3, and 69.0 correspond to the reflection from 100, 002, 101,102, 110, 103, 200, and 112 planes, respectively (Peng *et al*. 2010a). The XRD pattern of ZnO was modeled with the space group C6V=P63mc, which corresponds to hexagonal phase with wurtzite structure. After refinement, the R-$_{bragg}$ residue found for this structure was 12 %.

Table 1 Rietveld analysis of the ZnO phase; lattice parameters, average crystallite size, and the average microstrain.

Sample	Average size (nm)	Average microstrain (%)	Reported values in the ICDD-01-076-0704 (Å)	
			a = b	c
ZnO	74	0.31	3,2568	5,2125
			values obtained by refinement (Å)	
			a = b	c
			3,2559	5,2155

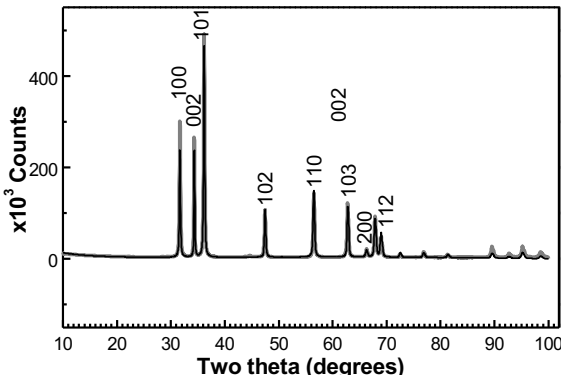

Fig. 3. Rietveld refinement plot of ZnO. The gray curve corresponds to the experimental data, and the black curve shows the calculated XRD pattern. The lower curve is the difference between both data sets. The vertical marks correspond to the ZnO phase.

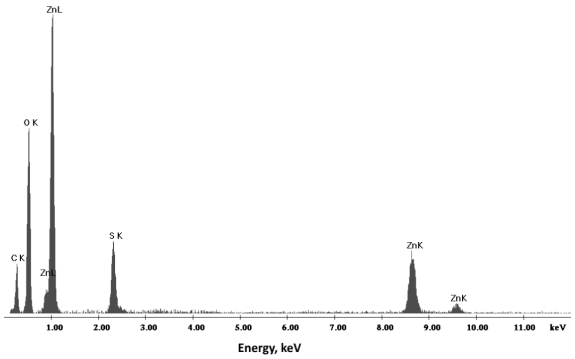

Fig. 4. EDS spectrum of ZnO microstructures.

Table 1 lists the lattice parameters, average crystallite size, and the average crystallite strain of the zinc oxide phase. The unit cell dimensions obtained by Rietveld refinement method (Romero-Galarza *et al*. 2014) are slightly different to the reported values in the ICDD-01-076-0704. A small decrease of the a-axis and a small increase of the c-axis were observed. Thus the change of the dimensions in the unit cell affects the ZnO crystallites morphology. Fig. 4 shows the elemental analysis obtained by EDS. It can be seen the typical peak corresponding to Zn and O. Carbon signal can be due to the grid used for sample analysis; however peak corresponding to S, can be ascribed to some SDS surfactant which remains after ZnO washing.

Fig. 5a shows a typical SEM image of the as-prepared ZnO nanostructures at 5,000 magnifications. Many six-blade impeller-like ZnO nanostructures are detected (circles). Observed diameters for this morphology were between 500 nm and 1 μm. However some others morphologies can be detected like needles with 300 to 600 nm in length. Upon 10,000 magnification agglomerated structures cabbage-like of approximately 2 μm of diameter were also observed as shown in Fig. 5b (squares). Fig. 5c shows also spherical particles having sizes of $\approx$ 25 nm of diameter and rice grain shape morphologies with average size of 50 nm in length. Structural details of the ZnO microparticles were analyzed by HR-TEM as shown in Fig. 5d. HR-TEM image displays clear lattice fringes, which reveal the single crystalline nature of ZnO. The measured lattice spacing was 0.28 nm, which is slightly different to the value of 0.2817 nm reported in the ICDD- 01-076-0704, corresponding to the (0001) planes, confirming that the ZnO nanoparticles are preferentially grown along [0001] direction, as well as the difference between both lattice spacing could be related to the micro-strain reported in Table 1.

According to methodology reported by Xie *et al*. (2011), needle-like morphology was expected, but in our case changing temperature of NaOH addition from 3 °C to room temperature, very different morphologies with smaller sizes were obtained. This behavior can be ascribed to better surfactant stabilization at higher temperatures. Crystal formation is divided in two steps: nucleation and growing, therefore its rates define ZnO morphology. Nucleation and growing rates are strongly affected by the presence of additives as SDS, basicity solution and temperature (Xie *et al*., 2011, Li *et al*., 2005). In our case we had used high OH^- concentration (ZN_2^+/OH^- molar ratio = 1:6), which would ensure the formation of a high number of nuclei; but in the other hand, it has been proposed that SDS can be absorbed at the ZnO nuclei on the 0001 crystal face, retarding the growth along c-axis.

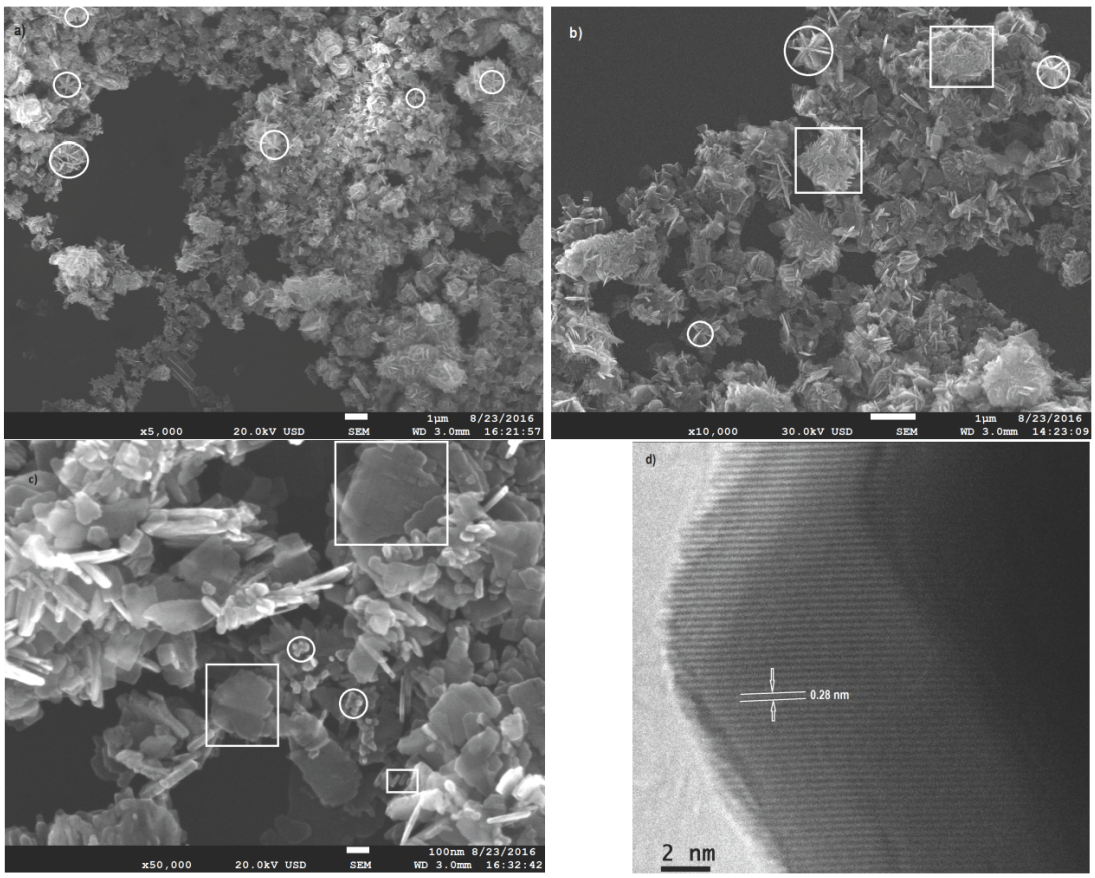

Fig. 5. SEM images (a-c) at different magnifications, and (d) HR-TEM of ZnO microstructures.

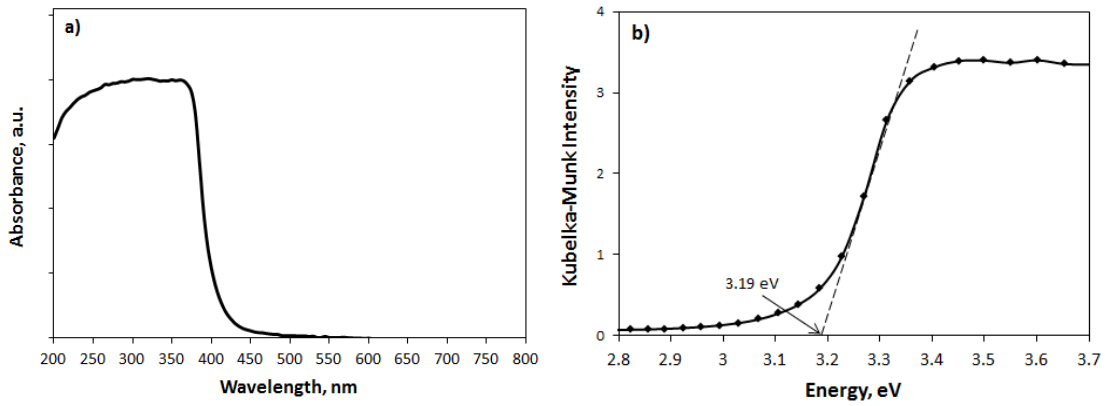

Fig. 6. UV/Vis-NIR absorption spectrum (a) and Kubelka-Munk function (b) of synthesized ZnO microparticles.

However, from our XRD and HR-TEM results we can conclude that the high number of formed nuclei favored the growth along [0001] crystal face.

The UV/Vis-NIR absorption spectra of the samples are shown in Fig. 6a. Synthesized ZnO microparticles showed a strong absorption band between 200 nm and 400 nm. The band gap energy of the sample was determined from extrapolation of the linear portion of the Kubelka-Munk data to the photon energy (hν) axis intercept (Cimitan *et al.*, 2009), as shown in Fig. 6b. The observed band gap of the sample was 3.19 eV.

Table 2 Some band gap values recently reported in the literature for ZnO nanostructures synthesized by different chemical routes and precursors.

Reference	Precursor	Morphology	Band gap, eV
Bijanzad *et al*. (2015)	Zinc nitrate	Mesoporous microbricks	3.19
Kumar *et al*. (2016)	Zinc acetate	Spherical	3.12
Kulkarni *et al*. (2015)	Zinc acetate	Spherical	3.30
Kumar *et al*. (2013)	Zinc sulfate	Nanoflakes	3.27-3.30a)
Samuel *et al*. (2009)	Zinc nitrate	Spherical	3.40
Moharram *et al*. (2014)	Zinc acetate	Spherical	3.52
Wang *et al*. (2012)	Zinc nitrate-ZnO_2	Spherical	3.0 to 3.25
This work	Zinc chloride	Impeller-, sheet-, and spherical-like	3.19

This value is slightly lower than some reported in the literature (Table 2). It can be seen in this Table that band gap observed in our case is the same reported value by Bijanzad *et al*. (2015) but higher than the value reported by Kumar *et al*. (2016). However, most of chemical routes involve a calcination step at high temperatures, which is avoided in our work.

Specific surface area BET-is affected by the morphology and size of microparticles. From N_2 physisorption analysis, it was observed that BET area of ZnO microparticles synthesized in this work was 26.5 m^2/g. This value agrees with that reported in the literature, for example, Thirumavalavan *et al*. (2013) synthesized ZnO spherical nanoparticles with diameters between 31 nm and 584 nm and BET areas in the range of 2.3 m^2/g to 23.7 m^2/g, depending on calcination temperature. Also, Bamiduro *et al*. (2014) obtained ZnO microrods by the hydrothermal method, observing very low BET surface area (2.8 m^2/g). Lee *et al*. (2014) found BET surface area as high as 233 m^2/g in the synthesis of ZnO nanoparticles by precipitation from zinc acetate in the presence of diethylene glycol and polyethylene glycol as stabilizing agents. Therefore, we can conclude that used method to synthesize ZnO microparticle strongly affects the specific surface area.

Conclusions

ZnO microstructures were prepared using a simple precipitation method at room temperature and aging at 80 °C. SEM images of ZnO showed that the main morphology was six-blade impeller-like and sheet-like and, in minor amounts rice grain-like and spherical morphologies. XRD analysis confirmed that the as prepared material has a high purity and EDS analysis showed the presence of S element due to some SDS remaining in trace level. The band gap of ZnO was 3.19 eV which is slightly lower than the average values reported in literature. BET area of ZnO microparticles synthesized in this work was 26.5 m^2/g.

Acknowledgments

This work was supported by SEP-PRODEP through Program [grant Red de Investigación y Desarrollo de Nanomateriales Híbridos para Aplicaciones Ambientales Avanzadas]. Author HMG acknowledges the support of the IPN through the project number 20160072.

References

Bamiduro, F., Ward, M.B., Brydson, R., Milne, S.J. (2014). Hierarchical growth of ZnO particles by a hydrothermal route. *Journal of the American Ceramic Society 97*, 1619-1624.

Banerjee, D., Lao, J.Y., Wang, D.Z., Huang, J.Y., Ren, Z.F., Steeves, D., Kimball, B., Sennett, M. (2003). Large-quantity free-standing ZnO nanowires. *Applied Physics Letters 83*, 2061-2063.

Bijanzad, K., Tadjarodi, A., Akhavan, O. (2015). Photocatalytic activity of mesoporous microbricks of ZnO nanoparticles prepared by the thermal decomposition of bis(2-aminonicotinato) zinc (II). *Chinese Journal of Catalysis 36*, 742-749.

Chen, J.C., Tang, C.T. (2007). Preparation and application of granular ZnO/Al_2O3 catalyst for the removal of hazardous trichloroethylene. *Journal of Hazardous Materials 142*, 88-96.

Chiu, W.S., Khiew, P.S., Cloke, M., Isa, D., Tan, T.K., Radiman, S., Abd-Shukor, R., Abd-Hamid, M.A., Huang, N.M., Lim, H.N., Chia, C.H. (2010). Photocatalytic study of two-dimensional ZnO nanopellets in the decomposition of methylene blue. *Chemical Engineering Journal 158*, 345-352.

Cimitan, S., Albonetti, S., Forni, L., Peri, F., Lazzari, D. (2009). Solvothermal synthesis and properties control of doped ZnO nanoparticles. *Journal of Colloid and Interface Science 329*, 73-80.

Filali, B.E., Torchynska, T.V. Díaz-Cano, A.I., Morales Rodriguez M. (2015). Structural and Raman scattering studies of ZnO Cu nanocrystals grown by spray pyrolysis. *Revista Mexicana de Ingeniería Química 14*, 781-788.

Grillo, R., Rosa, A.H., Fraceto, L.F. (2015). Engineered nanoparticles and organic matter: A review of the state-of-the-art. *Chemosphere 119*, 608-619.

Kolodziejczak-Radzimska, A., Jesionowski, T. (2014). Zinc Oxide-from synthesis to application: A review. *Materials 7*, 2833-2881.

Kong, X., Ding, Y., Yang, R., Wang, Z.L. (2004). Single-crystal nanorings formed by epitaxial self-coiling of polar-nanobelts. *Science 303*, 1348-1351.

Kulkarni, S.S, Shirsat, M.D. (2015). Optical and structural properties of zinc oxide nanoparticles. *International Journal of Advanced Research in Physical Science (IJARPS) 2*, 14-18.

Kumar, H., Rani, R. (2013). Structural and optical characterization of ZnO nanoparticles synthesized by microemulsion route. *International Letters of Chemistry, Physics and Astronomy 14*, 26-36.

Kumar, S., Thakur, A., Rangra, V.S., Sharma, S. (2016). Synthesis and use of low-band-gap ZnO nanoparticles for water treatment. *Arabian Journal for Science and Engineering 41*, 2393-2398.

Kumar, S.S., Venkateswarlu, P., Rao, V.R., Rao, G.N. (2013). Synthesis, characterization and optical properties of zinc oxide nanoparticles. *International Nano Letters 3*, 30. doi:10.1186/2228-5326-3-30.

Lee, S.-K., Kim, A.Y., Lee, J.Y., Ko, S.H., Kim, S.W. (2014). Facile synthesis of ZnO nanoparticles and their photocatalytic activity. *Bulletin of the Korean Chemical Society 35*, 2004-2008.

Li, P., Wei, Y., Liu, H., Wang, X.K. (2005). Growth of well-defined ZnO microparticles with additives from aqueous solution. *Journal of Solid State Chemistry 178*, 855-860.

Li, S., Gross, G.A., Günther, P.M., Köhler, J.M. (2011). Hydrothermal micro continuous-flow synthesis of spherical, cylinder-, star- and flower-like ZnO microparticles. *Chemical Engineering Journal 167*, 681-687.

Moharram, A.H., Mansour, S.A., Hussein, M.A., Rashad, M. (2014). Direct precipitation and characterization of ZnO nanoparticles. *Journal of Nanomaterials 2014*, 1-5. doi: 10.1155/2014/716210.

Nikoobakht, B., Wang, X., Herzing, A., Shi, J. (2013). Scalable synthesis and device integration of self-registered one-dimensional zinc oxide nanostructures and related materials. *Chemical Society Reviews 42*, 342-365.

Ovando-Medina, V.M., López, R.G., Castillo-Reyes, B.E., Alonso-Dávila, P.A., Martínez-Gutiérrez, H., González-Ortega, O., Farías-Cepeda, L. (2015). Composite of acicular rod-like ZnO nanoparticles and semiconducting polypyrrole photoactive under visible light irradiation for methylene blue dye photodegradation. *Colloid and Polymer Science 293*, 3459-3469.

Peng, Z., Dai, G., Chen, P., Zhang, Q., Wan, Q., Zou, B. (2010a). Synthesis, characterization and optical properties of star-like ZnO nanostructures. *Materials Letters 64*, 898-900.

Peng, Z,, Dai, G., Zhou, W., Chen, P., Wan, Q., Zhang, Q., Zou, B. (2010b). Photoluminescence and Raman analysis of novel ZnO tetrapod and multipod nanostructures. *Applied Surface Science 256*, 6814-6818.

Pereira, A.E., Grillo, R., Mello, N.F., Rosa, A.H., Fraceto, L.F. (2014). Application of poly(epsilon-caprolactone) nanoparticles containing atrazine herbicide as an alternative technique to control weeds and reduce damage to the environment. *Journal of Hazardous Materials 268*, 207-215.

Pérez-Sicairos, S., Miranda-Ibarra, S.A., Lin-Ho, S.W., Álvarez-Sánchez, J., Pérez-Reyes, J.C., Corrales-López, K.A., Morales-Cuevas, J.B. (2016). Membranas de nanofiltración, preparadas vía polimerización en interfase, dopadas con nanopartículas de ZnO: efecto en su desempeño. *Revista Mexicana de Ingeniería Química 15*, 961-975.

Romero-Galarza, A., Dahlberg, K.A., Chen, X., Schwank, J.W. (2014). Crystalline structure refinements and properties of Ni/TiO_2 and Ni/TiO_2-Ce catalysts and application to catalytic reaction of "CO + NO". *Applied Catalysis A: General 478*, 21-29.

Romo, L.E., Saade, H., Puente, B., López, M.A., Betancourt, R., López, R.G. (2011). Precipitation of zinc oxide nanoparticles in bicontinuous microemulsions. *Journal of Nanomaterials 2011*, 1-91. doi: 10.1155/2011/145963.

Samuel, M.S, Bose, L., George, K.C. (2009). Optical properties of ZnO nanoparticles. *Academic Review 16*, 57-65.

Thirumavalavan, M., Huang, K.-L., Lee, J.-F. (2013). Preparation and morphology studies of nano zinc oxide obtained using native and modified chitosans. *Materials 6*, 4198-4212.

Wahab, R., Ansari, S.G., Kim, Y.S., Seo, H.K., Shin, H.S. (2007). Room temperature synthesis of needle-shaped ZnO nanorods via sonochemical method. *Applied Surface Science 253*, 7622-7626.

Wang, J., Wang, Z., Huang, B., Ma. Y., Liu, Y., Qin, X., Zhang, X., Dai, Y. (2012). Oxygen vacancy induced band-gap narrowing and enhanced visible light photocatalytic activity of ZnO. *ACS Applied Material Interfaces 4*, 4024-4030. doi: 10.1021/am300835p.

Wu, J.J., Liu, S.C., Wu, C.T., Chen, K.H., Chenm, L.C. (2002). Heterostructures of ZnO-Zn coaxial nanocables and ZnO nanotubes. *Applied Physics Letters 81*, 1312-1314.

Xie, J., Li, Y., Zhao, W., Bian, L., Wei, Y. (2011). Simple fabrication and photocatalytic activity of ZnO particles with different morphologies. *Powder Technology 207*, 140-144.

Zamiri, R., Zakaria, A., Ahangar, H.A., Darroudi, M., Zak, A.K., Drummen, G.P.C. (2012). Aqueous starch as a stabilizer in zinc oxide nanoparticle synthesis via laser ablation. *Journal of Alloys and Compounds 516*, 41-48.